# New Pilot-Plant Photo-Fenton Solar Reactor for Water Decontamination

**Jorgelina Farias,[†] Enrique D. Albizzati,[‡] and Orlando M. Alfano*[,†]**

*Instituto de Desarrollo Tecnológico para la Industria Química (INTEC), Consejo Nacional de Investigaciones Científicas y Técnicas (CONICET) and Universidad Nacional del Litoral (UNL), Güemes 3450, 3000 Santa Fe, Argentina, and Facultad de Ingeniería Química, Universidad Nacional del Litoral (UNL), Santiago del Estero 2654, 3000 Santa Fe, Argentina*

A theoretical and experimental study of a new pilot-plant solar reactor for the photo-Fenton treatment of waters containing toxic organic compounds is presented. This hybrid unit was designed and built to capture thermal and photochemical solar radiation, yielding higher degradation rates of a model pollutant. The mass and thermal energy balances and the radiative transfer equation are solved to compute the pollutant and hydrogen peroxide concentrations and the reaction temperature as a function of time. The spectral UV/visible and broadband solar radiation incident on the reactor window are estimated from a computational code: the Simple Model for the Atmospheric Radiative Transfer of Sunshine (SMARTS2) program. Under irradiated runs, an experimental temperature increase up to 25 °C is reached. Also, for a reaction time of 180 min and a relatively low iron concentration, the combined effect of UV/visible and thermal sunlight is able to degrade 98.2% of the initial pollutant concentration.

## 1. Introduction

In recent years, the feasibility of applying sunlight has made the photo-Fenton process an economical and competitive method for the remediation of waters containing toxic and biologically nondegradable organic pollutants. Several attempts have been made to investigate the favorable effects of UV/visible solar radiation and/or the reaction temperature on the rate of the overall detoxification reaction. With these objectives, various aqueous organic compounds have been studied using solar degradation processes: 4-nitrophenol,[1] textile effluents,[2] cellulose bleaching effluents,[3] nonbiodegradable chlorinated solvents,[4] alachlor,[5] formic acid,[6] textile reactive dyes,[7] and a mixture of commercial pesticides,[8] among others.

It is known that the solar reactor performance can present a strong dependence on the radiation flux incident on the reactor window. Solar irradiance depends on season, geographic location, hour of day, and weather; consequently, these solar flux fluctuations with place and time should be considered in the evaluation of the pollutant degradation rate. For example, a "corrected illumination time" has been defined for comparing solar experiments performed with different solar reactors.[9−11] Another useful approach to evaluate the solar radiation flux incident on the reactor window as a function of time, in a given day and on different days of the year, is based on the application of simple, parametrized computational codes. These models can be employed to compute the direct normal and diffuse spectral solar radiation at the earth's horizontal or tilted surfaces, for different wavelength ranges. The simple solar spectral model SPCTRAL2, developed by Bird and Riordan,[12] has been applied to evaluate the direct and diffuse solar radiation at the reactor window, under cloudless atmospheres.[13] Afterward, Gueymard[14] proposed the Simple Model for the Atmospheric Radiative Transfer of Sunshine (SMARTS2) atmospheric transmittance model, a more accurate radiation model than SPCTRAL2 to predict the spectral distribution of the solar radiation at the earth's surface.[15,16] This model is based on a more detailed parametrization of the extinction processes in the atmosphere; more accurate absorption coefficients and temperature and relative humidity effects have been included. The SMARTS2 computational code has been applied to estimate the incoming radiation flux for different solar processes.[17−19]

Different solar reactors have been developed and tested in recent years to conduct photocatalytic processes for the treatment of polluted water.[20−22] An interesting process was proposed by Sagawe et al.,[1] based on a combination of photochemical and thermal utilization of solar energy to enhance the Fenton degradation rate of an organic pollutant. In the present work, a new solar reactor has been designed and built for the photo-Fenton treatment of pollutants in aqueous solution.[23] This pilot-plant photoreactor is a hybrid unit that captures the thermal and photochemical solar radiation. Figure 1 gives some details of the reactor.

In order to test the performance of this solar reactor, a theoretical and experimental study was performed using formic acid as a model contaminant. Regarding the pollutant employed in this study, formic acid has been frequently used as the target organic compound in several studies on advanced oxidation technologies. It is known that its reaction with hydroxyl radicals is fast and that it has a well-defined reaction mechanism.[24,25] On the other hand, this compound has a high solubility in water, does not produce a stable reaction byproduct, and is generally the final organic compound during degradation reactions of most of the organic pollutants before being finally mineralized to carbon dioxide.[26−29] The pollutant degradation rate under different experimental conditions was investigated, evaluating

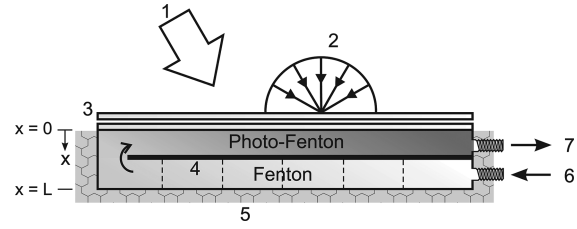


**Figure 1.** Details of the photo-Fenton solar reactor: 1, beam (direct) solar radiation; 2, diffuse solar radiation; 3, two-plate UV-transparent window; 4, absorbent plate; 5, thermal insulation; 6, inlet; 7, outlet.

* To whom correspondence should be addressed. Tel.: +54 342 4511546. Fax: +54 342 4511087. E-mail: alfano@intec.unl.edu.ar.
[†] INTEC, CONICET−UNL.
[‡] Facultad de Ingeniería Química, UNL.

10.1021/ie901377p 
Published on Web 12/18/2009

the species concentrations, reaction temperature, and UV and total broadband solar radiation fluxes as a function of time, applying the SMARTS2 computational code.

## 2. Reactor Model

**2.1. Local Volumetric Rate of Photon Absorption.** A complete radiation field model inside a nonconcentrating, flat-plate solar photoreactor has been proposed and experimentally verified in a previous work.[30] It was assumed that the glass window of the reactor was irradiated with direct and diffuse solar radiation, and that only radiation absorption in the reacting medium took place; i.e., radiation scattering and emission were neglected. A detailed analysis of the reflection, refraction, and absorption phenomena in the glass window was included. Afterward, these authors computed the local volumetric rate of photon absorption (LVRPA) and this radiation variable was used to predict the volume-averaged reaction rate of a well-known chemical actinometer (uranyl oxalate) for different actinometer initial concentrations and solar zenith angles. Similar expressions are applied in this work to predict the spectral LVRPA as a function of the spatial coordinate $x$ inside the reactor using the proper expressions to compute the direct and diffuse transmittances for the two-plate UV-transparent window (Figure 1).

The spectral LVRPA corresponding to the beam (or direct) solar radiation component is given by the expression

$$e^{a}_{B,\lambda}(x,t) = \kappa_\lambda(t)\, q_{B,\lambda}(t)\, Y_{B,\lambda}(\mu_i) \exp[-\kappa_{T,\lambda}(t)x/\mu_{ref}] \quad (1)$$

where $q_{B,\lambda}$ is the beam radiation flux for a given wavelength, $Y_{B,\lambda}$ is the beam transmittance, $\kappa_\lambda$ is the spectral volumetric absorption coefficient of the absorbing species, $\kappa_{T,\lambda}$ is the total absorption coefficient, and $\mu_{ref}$ and $\mu_i$ are the cosines of refraction and incident angles. The expression to calculate the spectral beam transmittance,[31] is

$$Y_{B,\lambda}(\mu_i) = \frac{Y_{1,\lambda}(\mu_i)\, Y_{2,\lambda}(\mu_i')}{1 - \mathscr{R}_{1,\lambda}(\mu_i)\, \mathscr{R}_{2,\lambda}(\mu_i')} \quad (2)$$

where $Y_{i,\lambda}$ and $\mathscr{R}_{i,\lambda}$ ($i = 1, 2$) are the direct transmittance and reflectance for each plate:

$$Y_{i,\lambda} = \frac{\tau_\lambda(\mu_{ref})(1-\rho_{nm})(1-\rho_{uv})}{1 - \tau_\lambda^{\,2}(\mu_{ref})\rho_{uv}\rho_{nm}} \quad (3)$$

$$\mathscr{R}_{i,\lambda} = \rho_{nm} + \frac{\tau_\lambda^{\,2}(\mu_{ref})(1-\rho_{nm})\rho_{uv}}{1 - \tau_\lambda^{\,2}(\mu_{ref})\rho_{uv}\rho_{nm}} \quad (4)$$

$$\tau_\lambda(\mu_{ref}) = \exp\left[-\kappa_\lambda(t)\frac{e}{\mu_{ref}}\right] \quad (5)$$

In eqs 3−5, $\rho_{nm}$ and $\rho_{uv}$ are the interface reflectivities and $e$ is the plate thickness.

The diffuse solar radiation component of the spectral LVRPA is given by

$$e^{a}_{D,\lambda}(x,t) = 2\kappa_\lambda(t)\, q_{D,\lambda}(t)\, Y_{D,\lambda} E[x, \kappa_\lambda(t)] \quad (6)$$

Here $q_{D,\lambda}$ is the diffuse radiation flux for a given wavelength, $Y_{D,\lambda}$ is the diffuse transmittance, and $E(x,t)$ is the second order exponential integral function. The spectral diffuse transmittance can be estimated as the spectral beam transmittance for a solar zenith angle equal to 60°:[32]

$$Y_D = Y_B[\mu_i = \cos(60°)] \quad (7)$$

Finally, substituting eqs 1 and 6 into eq 8, the spectral LVRPA corresponding to the total solar radiation is obtained:

$$e^{a}_{\lambda}(x,t) = e^{a}_{B,\lambda}(x,t) + e^{a}_{D,\lambda}(x,t) \quad (8)$$

**2.2. Kinetic Model.** Recently, Farias et al.[33] have proposed a kinetic model of the photo-Fenton degradation rates for relatively low iron concentrations, employing formic acid as a model pollutant. The reaction rate equations were derived considering an accepted reaction scheme with 14 reaction steps that involves initiation, propagation, and termination elementary reactions, and accounting for explicitly the expression of the spectral LVRPA.

The mathematical expressions derived in the quoted reference may be used to compute the formic acid ($R_F$), hydrogen peroxide ($R_P$), and ferrous ion ($R_{Fe^{2+}}$) degradation rates:

$$R_F(x,t) = R^T_F(t) - \frac{1}{\delta}\bar{\Phi}_{Fe(II)}\sum_\lambda e^{a}_\lambda(x,t) \quad (9)$$

with

$$R^T_F(t) = -C_P\frac{K_2 C_{Fe^{2+}}}{\delta} \quad (10)$$

$$R_P(x,t) = R^T_P(t) + \frac{1}{\delta}\left(1 - \frac{\gamma}{\xi}\right)\bar{\Phi}_{Fe(II)}\sum_\lambda e^{a}_\lambda(x,t) \quad (11)$$

with

$$R^T_P(t) = -C_P\frac{K_2 C_{Fe^{2+}}}{\delta}\left(\delta - 1 + \frac{\gamma}{\xi}\right) - C_P\frac{K_1 C_{Fe^{3+}}}{\xi} \quad (12)$$

$$R_{Fe^{2+}}(x,t) = R^T_{Fe^{2+}}(t) + \frac{2}{\delta}\frac{\gamma}{\xi}\bar{\Phi}_{Fe(II)}\sum_\lambda e^{a}_\lambda(x,t) \quad (13)$$

with

$$R^T_{Fe^{2+}}(t) = -2C_P\frac{K_2 C_{Fe^{2+}}}{\delta}\left(\delta - \frac{\gamma}{\xi}\right) + 2C_P\frac{K_1 C_{Fe^{3+}}}{\xi} \quad (14)$$

In eqs 9−14, the following dimensionless variables have been defined:

$$\gamma = K_3\frac{C_P}{C_F} + 1; \quad \delta = \gamma + K_4\frac{C_{Fe^{2+}}}{C_F}; \quad \xi = K_5\frac{C_{Fe^{2+}}}{C_{Fe^{3+}}} + 1 \quad (15)$$

In the previous equations, $R^T_F$, $R^T_P$, and $R^T_{Fe^{2+}}$ are the thermal degradation rates for the formic acid, hydrogen peroxide, and ferrous ion species, $C_F$, $C_P$, $C_{Fe^{2+}}$, and $C_{Fe^{3+}}$ are the formic acid, hydrogen peroxide, ferrous ion, and ferric ion concentrations, and $\bar{\Phi}_{Fe(II)}$ is the wavelength-averaged primary quantum yield. It should be also noted that the ferric ion concentration as a function of time may be determined from the initial ferric ion concentration ($C^0_{Fe^{3+}}$) and the actual ferrous ion concentration ($C_{Fe^{2+}}$).

The Arrhenius parameters $K_{\infty,i}$ and $E_i$, necessary to compute the kinetic parameters $K_i$ as a function of the reaction temperature (between 20 and 55 °C), were estimated applying a nonlinear, Newton Gauss−Marquardt optimization algorithm.[33] Values of the kinetic parameters employed in this work are reported in Table 1.

**2.3. Mass Balances.** The new pilot-plant solar reactor was placed inside the loop of a batch recycling system (Figure 2). The system is comprised by a solar reactor, a storage tank, a

**Table 1. Values of Kinetic Parameters**

| | parameter | value | units |
|---|---|---|---|
| preexponential factors | $K_{\infty,1}$ | $1.19 \times 10^{17}$ | $M^{-1}\ s^{-1}$ |
| | $K_{\infty,2}$ | $1.5 \times 10^{9}$ | $M^{-1}\ s^{-1}$ |
| | $K_{\infty,3}$ | 0.14 | |
| | $K_{\infty,4}$ | 7.77 | |
| | $K_{\infty,5}$ | 0.07 | |
| activation energies | $E_1$ | 112.86 | kJ $mol^{-1}$ |
| | $E_2$ | 46.76 | kJ $mol^{-1}$ |
| $\lambda$-averaged primary quantum yield | $\bar{\Phi}_{Fe(II)}$ | 0.21[a] | mol $einstein^{-1}$ |

[a] Bossman et al.[34]

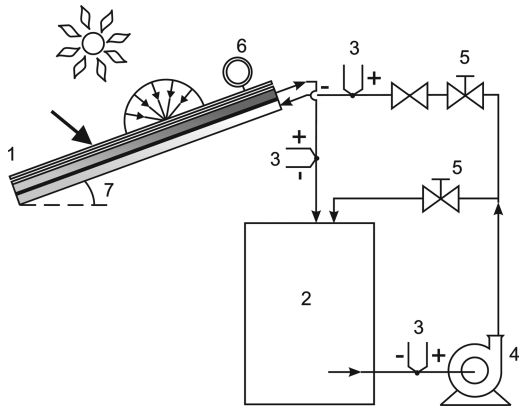


**Figure 2.** Schematic representation of the pilot-plant experimental setup: 1, solar reactor; 2, tank; 3, thermocouple; 4, pump; 5, valve; 6, radiometer; 7, tilt.

circulation pump, and tubing. The reactor entry aperture is tilted toward the north according to the latitude of Santa Fe city, Argentina.

The mass balances and the initial condition for a nonisothermal, well-stirred system are represented by the following matrix expressions:

$$\frac{\mathrm{d}}{\mathrm{d}t}\boldsymbol{C}(t) = \frac{V_{\mathrm{irr}}}{V}\langle \boldsymbol{R}(x,t)\rangle_{V_{\mathrm{irr}}} + \frac{V - V_{\mathrm{irr}}}{V}\boldsymbol{R^T}(t) \tag{16}$$

$$\boldsymbol{C}(t=0) = \boldsymbol{C^0} \tag{17}$$

The first term on the right-hand side of eq 16 gives the pollutant degradation produced by the photo-Fenton reaction that takes place in the irradiated liquid volume $V_{\mathrm{irr}}$ (upper channel, Figure 1). The second term on the right-hand side represents the contaminant decomposition generated by the thermal (or dark) reaction in the nonirradiated volume $V - V_{\mathrm{irr}}$ (lower channel, storage tank, and connecting lines between the tank and the reactor, Figure 2). The required reaction rate expressions to replace in eq 16 are given by eqs 9−14.

**2.4. Thermal Energy Balance.** Performing a thermal energy balance in the total reactor−tank system, the following ordinary differential equation is obtained:

$$C_{\mathrm{T}}\frac{\mathrm{d}T}{\mathrm{d}t} = \eta_{\mathrm{o}}A_{\mathrm{c}}q_{\mathrm{T}}(t) - (UA)_{\mathrm{R}}(T - T_{\mathrm{a}}(t)) - (UA)_{\mathrm{Tk}}(T - T_{\mathrm{a}}(t)) + Q_{\mathrm{P}} \tag{18}$$

Here $C_{\mathrm{T}}$ is the effective heat capacity of the reactor−tank system ($C_{\mathrm{T}} = C_{\mathrm{R}} + C_{\mathrm{Tk}}$), $T$ and $T_{\mathrm{a}}$ are the system and ambient air temperatures, $A_{\mathrm{c}}$ is the reactor window area, $q_{\mathrm{T}}$ is the total broadband solar radiation flux incident on the reactor wall, and $(UA)_{\mathrm{R}}$ and $(UA)_{\mathrm{Tk}}$ are the reactor and tank heat loss coefficients.

**Table 2. Pilot-Plant Solar Reactor Dimensions and Parameters**

| parameter | value | unit |
|---|---|---|
| reactor parameters | | |
| total liquid volume ($V$) | 35 | $dm^3$ |
| irradiated volume ($V_{\mathrm{irr}}$) | 6.1 | $dm^3$ |
| reactor depth ($L$) | 30 | mm |
| window area ($A_{\mathrm{c}}$) | 0.24 | $m^2$ |
| plate thickness ($e$) | 3.2 | mm |
| optical parameters | | |
| polycarbonate plate refractive index | 1.49 | |
| transmittance of acrylic windows | | |
| $\lambda = 300$ nm | 0.60 | |
| $\lambda = 350$ nm | 0.87 | |
| $\lambda = 360$ nm | 0.89 | |
| $\lambda = 373$ nm | 0.90 | |
| $\lambda = 400$ nm | 0.90 | |
| water refractive index | 1.33 | |
| air refractive index | 1.00 | |
| solar radiation parameters | | |
| UV/visible spectral range | [280:450] | nm |
| total radiation spectral range | [305:2800] | nm |
| tilt angle | 30 | deg |
| azimuth angle (counted clockwise from north) | 0 | deg |

In eq 18 the solar radiation absorbed per unit area of reactor window $A_{\mathrm{c}}$ is represented as the product of optical efficiency $\eta_{\mathrm{o}}$ times the total broadband incident radiation flux $q_{\mathrm{T}}$. The second and third terms are the thermal energy losses to the surroundings from the reactor and the tank, respectively; these are defined as the loss coefficient−area product ($UA$) and the difference between the temperature of the system $T$ and the ambient temperature $T_{\mathrm{a}}$. Finally, $Q_{\mathrm{P}}$ is the constant heat input from the circulation pump.

Defining the thermal energy parameters

$$\Omega = \frac{\eta_{\mathrm{o}}}{C_{\mathrm{T}}};\quad \Gamma = \frac{(UA)_{\mathrm{Tk}} + (UA)_{\mathrm{R}}}{C_{\mathrm{T}}};\quad \mathrm{K} = \frac{Q_{\mathrm{P}}}{C_{\mathrm{T}}} \tag{19}$$

we finally obtain the thermal energy balance and the initial condition used in this work to predict the temperature evolution in the solar reactor:

$$\frac{\mathrm{d}T}{\mathrm{d}t} = \Omega A_{\mathrm{c}}q_{\mathrm{T}}(t) - \Gamma(T - T_{\mathrm{a}}(t)) + \mathrm{K} \tag{20}$$

$$T = T^0;\quad t = 0 \tag{21}$$

## 3. Experimental Section

Based on the beneficial effect of solar energy to promote degradation of organic pollutants in aqueous solution, a pilot-plant solar reactor was built for photo-Fenton treatment. The newly designed nonconcentrating solar photoreactor is able to capture the UV/visible and near-infrared solar radiation. It is composed of a stainless steel, thermally insulated box with a two-plate acrylic window transparent to UV radiation and a black solar energy absorbing plate (Figure 1). The acrylic plates have a satisfactory mechanical resistance, a good outdoor durability under different atmospheric conditions, and a strong resistance to degradation caused by UV light.

The water to be treated enters the lower channel of the reactor and circulates in a zigzag pattern where it is preheated. Then the fluid goes into the upper channel where it absorbs UV/visible solar radiation and uses this radiation for the photochemical degradation of the pollutant. The complete reacting system is operated in a closed recirculating circuit driven by a high flow rate centrifugal pump and with a well-stirred reservoir tank. More details on the solar reactor dimensions and parameters can be found in Table 2.

**Table 3. Typical Experimental Runs for $C_F^0 = 3$ mM and Experimental and Predicted Results ($t = 180$ min)**

| no. | reaction | $C_{Fe^{3+}}^0$ (ppm) | $C_P^0/C_F^0$ | initial LST | run duration (h) | $T^0$ (°C) | $\Delta T$ (°C) | $X_F^{exp}$ (%) | $X_F^{pre}$ (%) | error (%) |
|---|---|---|---|---|---|---|---|---|---|---|
| 1 | irradiated | 1.8 | 1.5 | 10:30 | 3.5 | 25 | 18.2 | 66.2 | 66.5 | 0.4 |
| 2 | irradiated | 0.8 | 1.7 | 12:30 | 3.5 | 44[a] | 9.9 | 80.2 | 79.0 | 1.5 |
| 3 | irradiated | 3.4 | 2.2 | 12:30 | 3.5 | 32 | 15.7 | 98.2 | 99.1 | 0.9 |
| 4 | irradiated | 0.8 | 1.8 | 13:00 | 4.5 | 31 | 15.7 | 60.4 | 66.0 | 9.7 |
| 5 | irradiated | 0.8 | 3.1 | 10:50 | 4.5 | 27 | 16.6 | 75.8 | 72.0 | 5.0 |
| 6 | nonirradiated | 3.2 | 1.9 | 12:30 | 4.5 | 31 | 6.7 | 49.4 | 47.4 | 4.0 |

[a] Preheated solution.

To perform the experimental study of the pilot-plant solar reactor, the following working variables were modified (Table 3): (i) irradiated or nonirradiated condition, (ii) initial ferric ion concentration ($C_{Fe^{3+}}^0$), (iii) hydrogen peroxide to pollutant initial concentration ratio ($r$), (iv) initial local standard time (LST), (v) experimental run duration, and (vi) initial reaction temperature ($T^0$).

An experimental run started by covering the reactor window with an opaque plate to avoid the entrance of solar radiation. Then the pH was adjusted at 3.0 with concentrated sulfuric acid and the tank was filled with ferric sulfate (Carlo Erba, RPE) and formic acid (Merck, ACS) solutions. Afterward, the required amount of hydrogen peroxide solution (Carlo Erba, ACS, 30%) was added to the storage tank and the first sample was withdrawn; prior to analysis, the thermal reaction was suddenly quenched by adding sodium sulfite to the sample. The reactor cover was immediately removed to start the photo-Fenton reaction. Experimental runs were carried out during 210 or 270 min (see Table 3), and liquid sampling operation was repeated at equal time intervals. Once the run was completed, the total system was washed employing pure water.

Formic acid was analyzed with total organic carbon measurements (Shimadzu TOC-5000A), hydrogen peroxide employing a modified iodimetric technique,[35] and ferrous ions with a standard spectrophotometric method based on absorbance measurements of the Fe(II)−phenanthroline complex at 510 nm.

During the experimental runs, CUV3 and CM11 Kipp and Zonen radiometers mounted on a fixed-angle platform were employed to measure the UV and total broadband solar radiation fluxes incident on the two-plate reactor window. Also, type J thermocouples were used to measure the reaction temperature variations with time in different positions of the system (Figure 2).

## 4. Numerical Solution

To solve the equations of the proposed reactor model, the following computational steps must be considered for a constant solar zenith angle: (i) evaluation of the spectral direct and diffuse solar radiation incident at the two-plate UV-transparent window, (ii) computation of the spectral LVRPA as a function of position applying eqs 1−8, (iii) evaluation of the reaction rate for each one of the reactant species, eqs 9−15, and (iv) calculation of the reactant species concentrations and reaction temperatures as a function of time, solving the system of four nonlinear, first-order, ordinary differential equations defined by eqs 16 and 17 (mass balances for three species) and eqs 20 and 21 (thermal energy balance).

It should be stressed that the solar reactor model takes into account the variations of solar radiation with time (or with the solar zenith angle). To do this, the Simple Model for the Atmospheric Radiative Transfer of Sunshine (SMARTS2) code[14] was called in every loop of the numerical algorithm for solving the system of ordinary differential equations mentioned above. Figure 3 summarizes the algorithm developed for the resolution of the model equations.

The SMARTS2 predictions of the UV/visible and total solar radiation were obtained in Santa Fe city (31°39′ S, 60°43′ W, 8 m above sea level), Argentina, on an inclined north-facing surface.

Meteorological parameters such as the ground-level air temperature, the relative humidity, and the surface pressure were obtained at Centro de Informaciones Meteorológicas, Facultad de Ingeniería y Ciencias Hídricas, UNL.

Values of the ozone total column corresponding to each day of the experimental runs were taken from the information provided by the Total Ozone Mapping Spectrometer (TOMS)/NASA instrument on board the Earth Probe satellite.

Precipitable water vapor was calculated from empirical relationships, using measurements of the surface temperature and humidity.[14]

The Angstrom turbidity formula was applied to estimate the absorption and scattering by aerosols. Values of turbidity coefficients ($\beta$) equal to 0.02 and 0.07, corresponding to a clean sky, were assumed. The wavelength exponents for the Angstrom approach ($\alpha_1$ and $\alpha_2$), related to the size distribution of the aerosol particles, were adopted from a reference rural-aerosol model tabulated for different relative humidities.[14]

A value of 0.815 was adopted for the aerosol single scattering albedo for the UV/visible wavelength range (280−450 nm), and a value of 0.95 for the total wavelength range.[36] An aerosol asymmetry factor equal to 0.65 was assumed for any wavelength.[12]

A concrete ground cover was considered to estimate the local spectral albedo and to calculate the reflected solar radiation on the tilted plane.

It should be emphasized that the rural aerosol reference parameters, as well as the surface pressure, the air temperature, and the relative humidity, were modified for each time interval in the numerical resolution of the mass and thermal energy equations.

## 5. Pilot-Plant Scale Results

**5.1. Estimation of Thermal Energy Parameters.** Thermal energy parameters $\Omega$, $\Gamma$, and K, involved in eq 20, were estimated from measurements of the total broadband solar radiation flux incident on the reactor wall, the ambient air temperature, and the temperature variations in the storage tank, from a set of irradiated and nonirradiated experimental runs without chemical reaction. The temperatures in the storage tank obtained at different times were compared with simulation results. A nonlinear regression algorithm was then applied in order to provide the values of the three parameters that minimize the differences between predicted and measured temperatures. Values of these thermal energy parameters, with the corresponding 95% confidence interval, are reported in Table 4.

Figure 4 depicts the measured values as a function of time of the total broadband solar radiation (Figure 4a) and the ambient air temperature (Figure 4b), and the measured (symbols) and predicted (lines) values of the temperatures in the storage tank

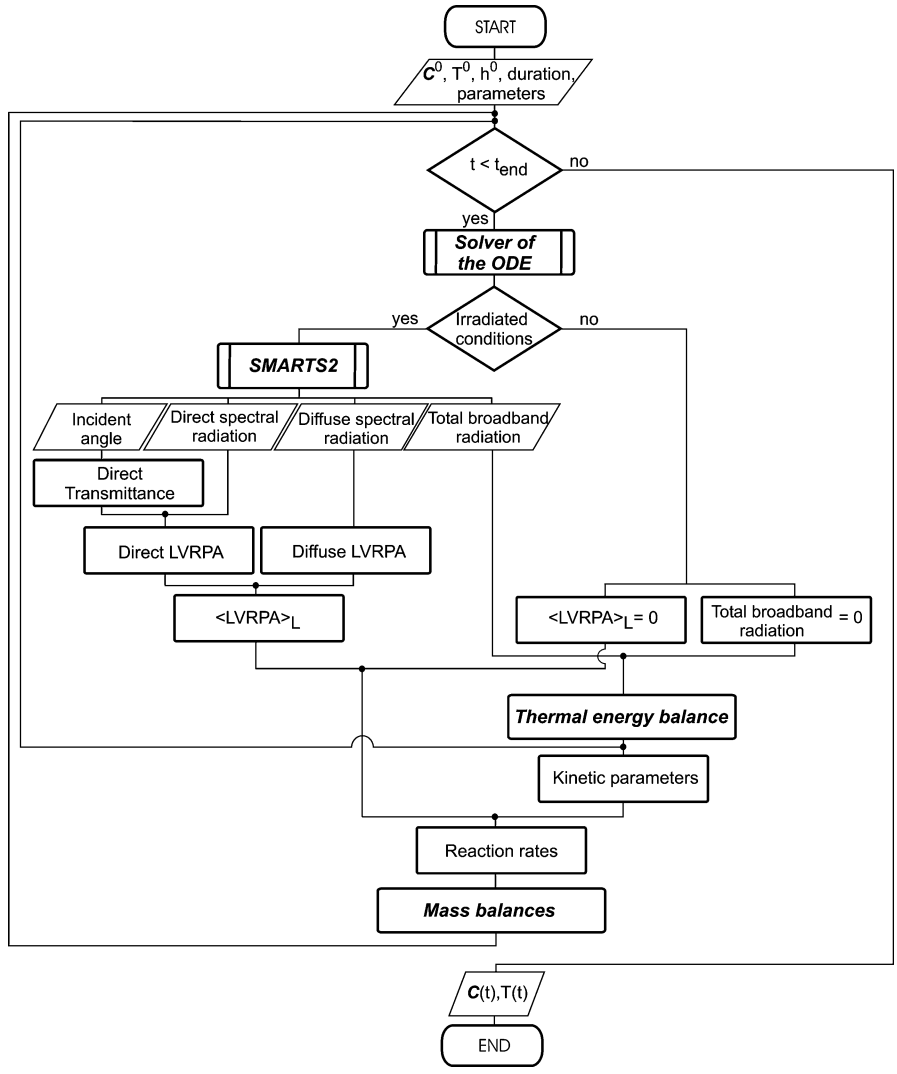


**Figure 3.** Flow diagram of the calculation procedure.

**Table 4. Estimated Values of Thermal Energy Balance Parameters**

| parameter | value | confidence interval (95%) | units |
|---|---|---|---|
| Ω | $9.10 \times 10^{-5}$ | $\pm 0.51 \times 10^{-5}$ | °C J$^{-1}$ |
| Γ | $5.39 \times 10^{-6}$ | $\pm 0.24 \times 10^{-6}$ | s$^{-1}$ |
| K | $8.28 \times 10^{-4}$ | $\pm 0.40 \times 10^{-4}$ | °C s$^{-1}$ |

(Figure 4c), under different operating conditions. Considering all the irradiated and nonirradiated runs, a good representation of the measured temperatures in the tank was obtained; the normalized root-mean-square error (NRMSE) of the estimations was 1.2%. It should be also noted that at the end of the irradiated runs (480 min) an experimental temperature increase up to 25 °C was obtained with this new pilot-plant solar reactor. Conversely, an increase of temperature no more than 10 °C was observed under nonirradiated conditions.

**5.2. Pollutant Degradation.** Figures 5, 6, and 7 show model predictions and experimental data as a function of time, for different operating conditions of the pilot-plant solar reactor and various days of the year. The following results are depicted in these figures: (i) pollutant, hydrogen peroxide, and ferrous ion concentrations, (ii) reaction temperatures, (iii) UV solar radiation fluxes, and (iv) total broadband solar radiation fluxes. After a reaction time of 180 min, Table 3 also shows the reaction temperature increase ($\Delta T$), the experimental and predicted contaminant conversions ($X_F^{exp}$ and $X_F^{pre}$), and the percent errors between model predictions and experimental data of the pollutant conversion.

Irradiated and nonirradiated experimental conditions are compared in Figure 5 (typical runs 1 and 6 in Table 3). These experiments were performed for a constant initial pollutant concentration ($C_F^0 = 3$ mM) and different initial ferric ion concentrations ($C_{Fe^{3+}}^0 = 1.8$ and 3.2 ppm), hydrogen peroxide to pollutant initial molar ratios ($r = 1.5$ and 1.9), and initial reaction temperatures ($T^0 = 25$ and 31 °C). Despite the lower values of $C_{Fe^{3+}}^0$, $r$, and $T^0$ employed for run 1, it can be seen from Figure 5a that the pollutant conversions under irradiated experiments are always higher than the ones obtained under nonirradiated conditions. After 180 min of operation, the pollutant conversion with the irradiated reactor is 66.2% versus 49.4% for the dark reactor. Significant differences in the temperature increase at the end of the runs are also observed in these experiments showing the effect of the infrared solar radiation on the reacting solution (Figure 5b); thermal solar radiation is able to increase the experimental temperature up to 20 °C after 210 min, compared with an increase of 8 °C reached under dark conditions at $t = 270$ min. Important variations are also reached in the contaminant conversions at the end of runs 1 and 6 (Figure 5a); under irradiated conditions the pollutant conversion was 76% at $t = 210$ min, compared with a conversion of only 59% under dark conditions at $t = 270$ min.

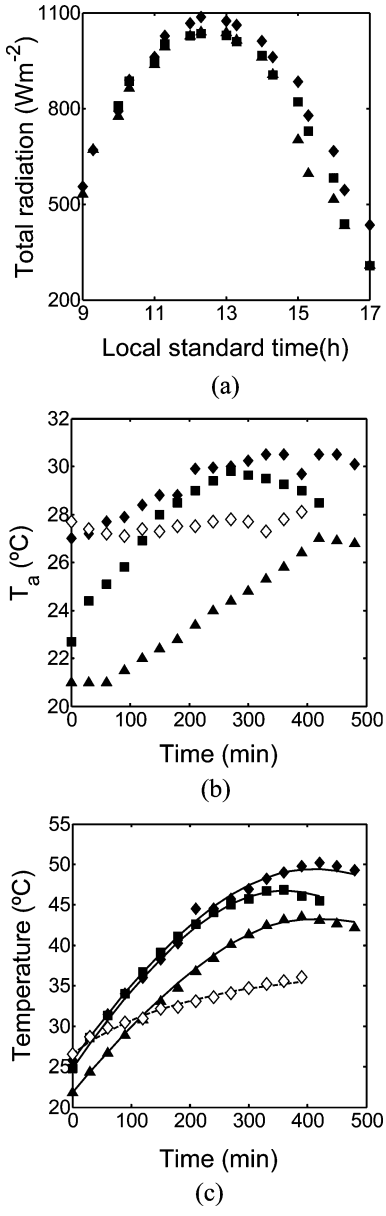


**Figure 4.** (a) Measured total broadband solar radiation, (b) measured ambient air temperature, (c) measured (symbols) and predicted (lines) temperatures in the storage tank. Irradiated (—, ◆, ■, ▲) and nonirradiated (---, ◇) experiments.

Figure 6 shows two irradiated experiments, corresponding to typical runs 1 and 4 in Table 3, carried out under a constant initial pollutant concentration ($C_F^0 = 3$ mM), low values of the initial ferric ion concentrations ($C_{Fe^{3+}}^0 = 1.8$ and 0.8 ppm), similar ratios of hydrogen peroxide to pollutant initial concentration ($r = 1.5$ and 1.8), and different initial reaction temperatures ($T^0 = 25$ and 31 °C). As can be seen in the figure, one of the runs was initiated before solar noon (run 1: initial LST 10:30) and the other one was initiated after solar noon (run 4: initial LST 13:00). For run 1, it is noted that the combined effect of UV/visible and thermal sunlight is able to increase the experimental temperature up to 18.2 °C and to degrade 66.2% of the initial pollutant concentration at $t = 180$ min. For run 4, in spite of the low initial ferric ion concentration (0.8 ppm) and the lower UV and total solar radiation fluxes measured at $t = 180$ min (Figure 6c,d), a pollutant conversion of 60.4% is reached. When experimental results between runs 1 and 4 are compared (Figure 6), it is worth noting that the higher level in the reaction temperature reached during run 4 is sufficient to

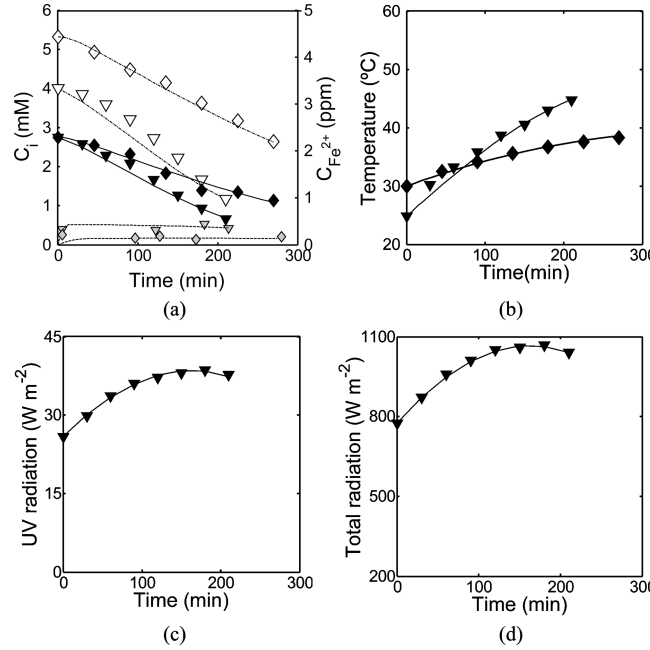


**Figure 5.** Model predictions (lines) and experimental data (symbols) vs time for $C_F^0 = 3$ mM. Keys for run 1, irradiated experiment: (—, ▼), $C_{Fe^{3+}}^0 = 1.8$ ppm, $\boldsymbol{R} = 1.5$, $T^0 = 25$ °C. Run 6, nonirradiated experiment: (—, ◆), $C_{Fe^{3+}}^0 = 3.2$ ppm, $r = 1.9$, $T^0 = 31$ °C. Compound concentrations: formic acid (—, ▼, ◆), hydrogen peroxide (— • —, ▽, ◇), and ferrous ion (---, gray downward pointing triangle, gray diamond).

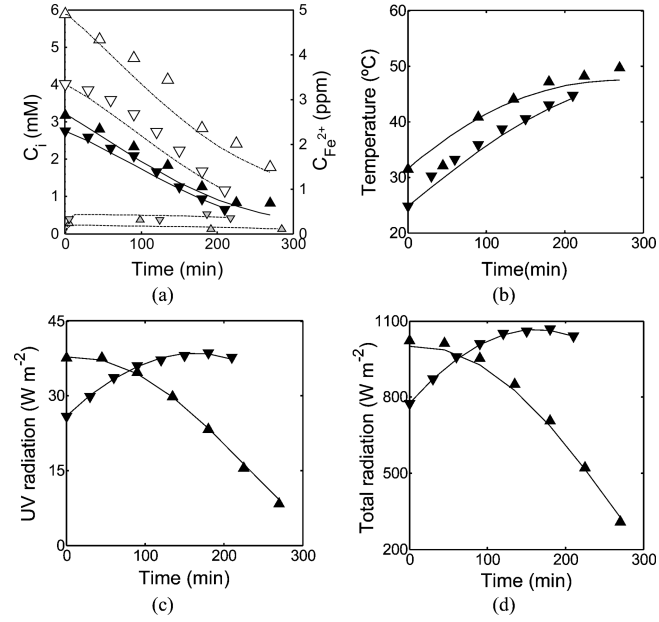


**Figure 6.** Model predictions (lines) and experimental data (symbols) vs time for $C_F^0 = 3$ mM. Run 1: (—, ▼), $C_{Fe^{3+}}^0 = 1.8$ ppm, $\boldsymbol{R} = 1.5$, $T^0 = 25$ °C. Run 4: (—, ▲), $C_{Fe^{3+}}^0 = 0.8$ ppm, $r = 1.8$, $T^0 = 31$ °C. Compound concentrations: formic acid (—, ▼, ▲), hydrogen peroxide (— • —, ▽, ◇), and ferrous ion (---, gray downward pointing triangle, gray upward pointing triangle).

compensate the significant reduction of the UV/visible and thermal solar radiation observed for this run after solar noon. Also, a similar beneficial effect of the reaction temperature level can be detected in typical run 2 (Table 3), where reaction temperatures higher than 44 °C are obtained employing a preheated solution; in this run, using the lowest ferric ion concentration, a pollutant conversion of 80.2% was reached after a reaction time of 180 min.

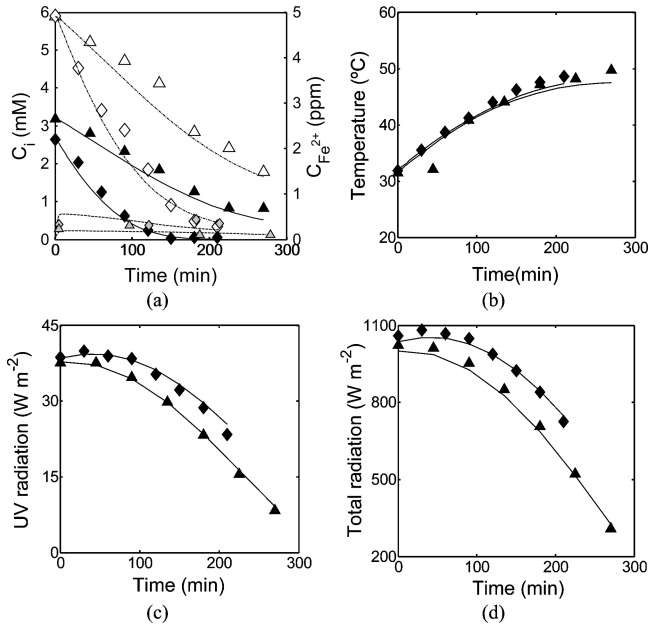


**Figure 7.** Model predictions (lines) and experimental data (symbols) vs time for $C_F^0 = 3$ mM. Run 3: (—, ◆), $C_{Fe^{3+}}^0 = 3.4$ ppm, $\boldsymbol{R} = 2.2$, $T^0 = 32$ °C. Run 4: (—, ▲), $C_{Fe^{3+}}^0 = 0.8$ ppm, $r = 1.8$, $T^0 = 31$ °C. Compound concentrations: formic acid (—, ◆, ▲), hydrogen peroxide (— • —, ◇, △), and ferrous ion (---, gray diamond, gray downward pointing triangle).

The influence of the initial ferric ion concentration on the pilot-plant reactor performance was studied in the typical runs 3 and 4 (Figure 7). These experiments were carried out for a constant initial pollutant concentration ($C_F^0 = 3$ mM), two different initial ferric ion concentrations ($C_{Fe^{3+}}^0 = 3.4$ and 0.8 ppm), two hydrogen peroxide to pollutant initial molar ratios ($r = 2.2$ and 1.8), and similar initial reaction temperatures ($T^0 = 32$ and 31 °C). For a reaction time of 180 min and a relatively low ferric iron concentration (3.4 ppm), it should be noted that the combined effect of UV/visible and thermal solar radiation can degrade 98.2% of the initial contaminant concentration. Moreover, with the lowest ferric iron concentration (0.8 ppm), the organic pollutant conversion is at least 60.4%. At the end of these typical runs, the following pollutant conversions are observed (Figure 7a): $X_F(210\ \text{min}) = 99\%$ for run 3 ($C_{Fe^{3+}}^0 = 3.4$ ppm) and $X_F(270\ \text{min}) = 74\%$ for run 4 ($C_{Fe^{3+}}^0 = 0.8$ ppm). In this case, it should be noted that similar temperature increases are reached: 16.7 and 18.2 °C, respectively.

Figures 5a, 6a, and 7a also show hydrogen peroxide and ferrous iron concentrations as a function of time, under different operating conditions of the pilot-plant solar reactor. Due to the very low ferrous iron concentrations obtained in these runs, ppm units are used for iron concentrations on the right scale of these figures. It should be noted that, considering all the irradiated and nonirradiated runs, a good representation of the experimental results was obtained; the NRMSE of the model predictions was 10.2% for formic acid, 9.4% for hydrogen peroxide, 2.9% for reaction temperature, 3.7% for UV solar radiation flux, and 4.2% for total broadband solar radiation flux.

As shown from the previous experimental tests performed with this new pilot-plant solar reactor, very high pollutant conversions are reached under specific operating conditions. This good performance for pollutant removal from contaminated water can be achieved as a result of the combined utilization of the ultraviolet and thermal solar energy.

## 6. Conclusions

A new pilot-plant solar reactor has been designed and built for the photo-Fenton treatment of pollutants in aqueous solution. This hybrid solar unit is able to capture photochemical and thermal solar radiation increasing the degradation rate of a model compound.

The Simple Model for the Atmospheric Radiative Transfer of Sunshine (SMARTS2) computational code was applied to estimate the spectral UV/visible and total broadband solar radiation fluxes as a function of time in a given day and at different days of the year. To take into account the variations of solar radiation with the solar zenith angle, the SMARTS2 code was called in every loop of the numerical algorithm for solving the mass and thermal energy balance equations.

A theoretical and experimental study was performed to investigate the solar reactor performance using formic acid as a model pollutant. In order to compute the organic pollutant and hydrogen peroxide concentrations and the reaction temperature as a function of time, the mass and thermal energy balances and the radiative transfer equation were solved.

Under irradiated and nonirradiated experiments without chemical reaction, the thermal energy parameters necessary to solve the thermal energy balance were estimated from measurements of the total broadband solar radiation on the reactor window, the ambient air temperature, and the temperature variations in the tank.

For irradiated experimental runs, the reaction temperature in the system was increased up to 25 °C. Also, for a reaction time of 180 min and an initial ferric ion concentration of 3.4 ppm, the combined effect of UV/visible and thermal solar irradiation was able to degrade 98.2% of the initial pollutant concentration. When a very low iron concentration (0.8 ppm) was used, an organic pollutant conversion of 60% was reached.

## Acknowledgment

The authors are grateful to Universidad Nacional del Litoral (UNL), Consejo Nacional de Investigaciones Científicas y Técnicas (CONICET) and Agencia Nacional de Promoción Científica y Tecnológica (ANPCyT). They also thank Tec. Antonio C. Negro for his valuable help during the experimental work.

## Nomenclature

$A_c$ = window area, $m^2$
$C$ = molar concentration, M; also effective heat capacity, J $°C^{-1}$
$E$ = activation energy, kJ $mol^{-1}$
$e$ = plate thickness, mm
$e^a$ = local volumetric rate of photon absorption (LVRPA), Einstein $cm^{-3}$ $s^{-1}$
$K$ = kinetic parameter, $M^{-1}$ $s^{-1}$ ($K_1$ and $K_2$), dimensionless ($K_3$, $K_4$, and $K_5$)
$K_\infty$ = preexponential factor, $M^{-1}$ $s^{-1}$ ($K_{\infty,1}$ and $K_{\infty,2}$), dimensionless ($K_{\infty,3}$, $K_{\infty,4}$, and $K_{\infty,5}$)
$L$ = reactor depth, mm
$Q_P$ = heat input from the pump, J $s^{-1}$
$q$ = net solar radiation flux, Einstein $m^{-2}$ $s^{-1}$
$\mathscr{R}$ = reflectance, dimensionless
$R$ = reaction rate, M $s^{-1}$
$T$ = temperature, °C
$t$ = time, s
$V$ = volume, $dm^3$
$UA$ = heat loss coefficient−area product, J $°C^{-1}$ $s^{-1}$

$X$ = conversion, dimensionless
$x$ = spatial coordinate, m

*Greek Symbols*

$\gamma$ = function defined in eq 15, dimensionless
$\delta$ = function defined in eq 15, dimensionless
$\kappa$ = volumetric absorption coefficient, $m^{-1}$
$\eta_o$ = optical efficiency, dimensionless
$\lambda$ = wavelength, nm
K = ratio of heat input from the pump to effective heat capacity, °C $s^{-1}$
$\xi$ = function defined in eq 15, dimensionless
$\mu$ = quantity cos $\theta$
$\rho$ = reflectivity, dimensionless
$\tau$ = variable defined in eq 5, dimensionless
Y = transmittance, dimensionless
$\Gamma$ = ratio of heat loss to effective heat capacity, $s^{-1}$
$\Phi$ = primary quantum yield, mol $Einstein^{-1}$
$\Omega$ = ratio of optical efficiency to effective heat capacity, °C $J^{-1}$

*Subscripts*

a = air property
B = relative to beam (or direct) radiation
D = relative to diffuse radiation
F = relative to formic acid
$Fe^{2+}$ = relative to ferrous ion
$Fe^{3+}$ = relative to ferric ion
i = incident radiation
irr = relative to an irradiated property
P = relative to hydrogen peroxide
ref = refracted radiation
R = relative to the reactor
T = total
Tk = tank property
$\lambda$ = indicates a dependence on wavelength

*Superscripts*

exp = experimental value
0 = initial condition
pre = predicted value
T = thermal rate

*Special Symbols*

$\langle\ \rangle$ = average value

## Literature Cited


(1) Sagawe, G.; Lehnard, A.; Luübber, M.; Bahnemann, D. The Insulated Solar Fenton Hybrid Process: Fundamental Investigations. *Helv. Chim. Acta* **2001**, *84*, 3742.

(2) Pérez, M.; Torrades, F.; Domènech, X.; Peral, J. Fenton and Photo-Fenton Oxidation of Textile Effluents. *Water Res.* **2002**, *36*, 2703.

(3) Torrades, F.; Pérez, M.; Mansilla, H. D.; Peral, J. Experimental Design of Fenton and Photo-Fenton Reactions for the Treatment of Cellulose Bleaching Effluents. *Chemosphere* **2003**, *53*, 1211.

(4) Malato, S.; Blanco, J.; Maldonado, M. I.; Fernández-Ibáñez, P.; Gernjak, W.; Oller, I. Treatment of Chlorinated Solvents by $TiO_2$ Photocatalysis and Photo-Fenton: Influence of Operating Conditions in a Solar Pilot Plant. *Chemosphere* **2005**, *58*, 391.

(5) Gernjak, W.; Fuerhacker, M.; Fernández-Ibañez, P.; Blanco, J.; Malato, S. Solar Photo-Fenton Treatment—Process Parameters and Process Control. *Appl. Catal., B* **2006**, *64*, 121.

(6) Farias, J.; Rossetti, G. H.; Albizzati, E. D.; Alfano, O. M. Solar Degradation of Formic Acid: Temperature Effects on Photo-Fenton Reaction. *Ind. Eng. Chem. Res.* **2007**, *46*, 7580.

(7) García-Montaño, J.; Pérez-Estrada, L.; Oller, I.; Maldonado, M.; Torrades, F.; Peral, J. Pilot Plant Scale Reactive Dyes Degradation by Solar Photo-Fenton and Biological Processes. *J. Photochem. Photobiol., A* **2008**, *195*, 205.

(8) Zapata, A.; Velegraki, T.; Sánchez-Pérez, J. A.; Mantzavinos, D.; Maldonado, M. I.; Malato, S. Solar Photo-Fenton Treatment of Pesticides in Water: Effect of Iron Concentration on Degradation and Assessment of Ecotoxicity and Biodegradability. *Appl. Catal., B* **2009**, *88*, 448.

(9) Gernjak, W.; Maldonado, M. I.; Malato, S.; Cáceres, J.; Krutzler, T.; Glaser, A.; Bauer, R. Pilot-Plant of Olive Mill Wastewater (OMW) by Solar $TiO_2$ Photocatalysis and Solar Photo-Fenton. *Sol. Energy* **2004**, *77*, 567.

(10) Gomes, A. I.; Santos, J. C.; Vilar, V. J. P.; Boaventura, R. A. R. Inactivation of Bacteria E. Coli and Photodegradation of Humic Acids using Natural Sunlight. *Appl. Catal., B* **2009**, *88*, 283.

(11) Malato, S.; Blanco, J.; Videla, A.; Richter, C. Photocatalysis with Solar Energy at a Pilot-Plant Scale: an Overview. *Appl. Catal., B* **2002**, *37*, 1.

(12) Bird, R. E.; Riordan, C. Simple Spectral Model for Direct and Diffuse Irradiance on Horizontal and Tilted Planes at the Earth's Surface for Cloudness Atmospheres. *J. Clim. Appl. Meteorol.* **1986**, *25*, 87.

(13) Rossetti, G. H.; Albizzati, E. D.; Alfano, O. M. Modeling of a Flat-Plate Solar Reactor. Degradation of Formic Acid by the Photo-Fenton Reaction. *Sol. Energy* **2004**, *5*, 443.

(14) Gueymard, C. *SMARTS2, a Simple Model of the Atmospheric Transfer of Sunshine: Algorithms and Performance Assessment*; Report FSEC-PF-270-95; Florida Solar Energy Center: Cocoa, FL, 1995.

(15) Utrillas, M. P.; Boscá, J. V.; Martínez-Lozano, J. A.; Cañada, J.; Tena, F.; Pinazo, J. M. A Comparative Study of SPECTRAL2 and SMARTS2 Parameterised Models based on Spectral Irradiance Measurements at Valencia, Spain. *Sol. Energy* **1998**, *63*, 161.

(16) Tadros, M. T. Y.; El-Metwally, M.; Hamed, A. B. A Comparative Study on SPCTRAL2, SPCTR-1881 and SMARTS2 Models Using Direct Normal Irradiance in Different Bands for Cairo and Aswan, Egypt. *J. Atmosph. Solar Terr. Phys.* **2005**, *67*, 1343.

(17) Schlegel, G. O.; Burkholder, F. W.; Klein, S. A.; Beckman, W. A.; Wood, B. D.; Muhs, J. D. Analysis of a Full Spectrum Hybrid Lighting System. *Sol. Energy* **2004**, *76*, 359.

(18) Stubbins, A.; Uher, G.; Law, C. S.; Mopper, K.; Robinson, C.; Upsill-Goddard, R. C. Open-Ocean Carbon Monoxide Photoproduction. *Deep-Sea Res., II* **2006**, *53*, 1695.

(19) Werner, J. J.; McNeill, K.; Arnold, W. A. Environmental Photodegradation of Mefenamic Acid. *Chemosphere* **2005**, *58*, 1339.

(20) Bahnemann, D. Photocatalytic Water Treatment: Solar Energy Applications. *Sol. Energy* **2004**, *77*, 445.

(21) Blanco, J.; Malato, S.; Fernández-Ibañez, P.; Alarcón, D.; Gernjak, W.; Maldonado, M. Review of Feasible Solar Energy Applications to Water Processes. *Renew. Sustain. Energy Rev.* **2009**, *13*, 1437.

(22) Malato, S.; Blanco, J.; Alarcón, D.; Maldonado, M.; Fernández-Ibáñez, P.; Gernjak, W. Photocatalytic Decontamination and Disinfection of Water with Solar Collectors. *Catal. Today* **2007**, *122*, 137.

(23) Farias, J.; Rossetti, G. H.; Albizzati, E. D.; Alfano, O. M. Reactor Solar para Descontaminación de Aguas. Argentine Patent Office P-080103697, Aug 26, 2008.

(24) Duesterberg, C. K.; Cooper, W. J.; Waite, T. D. Fenton-Mediated Oxidation in the Presence and Absence of Oxygen. *Environ. Sci. Technol.* **2005**, *39*, 5052.

(25) Kwan, W. P.; Voelker, V. M. Decomposition of Hydrogen Peroxide and Organic Compounds in the Presence of Dissolved Iron and Ferrihydrite. *Environ. Sci. Technol.* **2002**, *36*, 1467.

(26) Araña, J.; González Díaz, O.; Miranda Saracho, M.; Doña Rodríguez, J. M.; Herrera Melián, J. A.; Pérez Peña, J. Photocatalytic Degradation of Formic Acid using $Fe/TiO_2$ Catalysts: the Role of $Fe^{3+}$/$Fe^{2+}$ Ions in the Degradation Mechanism. *Appl. Catal., B* **2001**, *32*, 49.

(27) Brillas, E.; Baños, M. A.; Garrido, J. A. Mineralization of Herbicide 3,6-dichloro-2-methoxybenzoic Acid in Aqueous Medium by Anodic Oxidation, Electro-Fenton and Photoelectro-Fenton. *Electrochim. Acta* **2003**, *48*, 1697.

(28) Huanga, Y.; Huanga, Y.; Changa, P.; Chena, Ch. Comparative Study of Oxidation of Dye-Reactive Black B by Different Advanced Oxidation Processes: Fenton, Electro-Fenton and Photo-Fenton. *J. Hazard. Mater.* **2008**, *154*, 655.

(29) Zazo, J. A.; Casas, J. A.; Mohedano, A. F.; Gilarranz, M. A.; Rodríguez, J. J. Chemical Pathway and Kinetics of Phenol Oxidation by Fenton's Reagent. *Environ. Sci. Technol.* **2005**, *39*, 9295.

(30) Rossetti, G.; Albizzati, E.; Alfano, O. Modeling and Experimental Verification of a Flat-Plate Solar Photoreactor. *Ind. Eng. Chem. Res.* **1998**, *37*, 3592.

(31) Siegel, R.; Howell, J. R. *Thermal Radiation Heat Transfer*, 4th ed.; Taylor & Francis: Washington, DC, 2002.

(32) Duffie, J. A.; Beckman, W. *Solar Engineering of Thermal Processes*, 2nd ed.; John Wiley & Sons: New York, 1991.

(33) Farias, J.; Albizzati, E.; Alfano, O. Kinetic Study of the Photo-Fenton Degradation of Formic Acid. Combined Effects of Temperature and Iron Concentration. *Catal. Today* **2009**, *144*, 117.

(34) Bossmann, S.; Oliveros, E.; Göb, S.; Siegwart, S.; Dahlen, E.; Payawan, L.; Straub, M., Jr.; Wörner, M.; Braun, A. New Evidence against Hydroxyl Radicals as Reactive Intermediates in the Thermal and Photochemically Enhanced Fenton Reactions. *J. Phys. Chem. A* **1998**, *102*, 5542.

(35) Allen, A. O.; Hochanadel, J. A.; Ghormley, J. A.; Davis, T. W. Decomposition of Water and Aqueous Solutions under Mixed Fast Neutron and Gamma Radiation. *J. Phys. Chem.* **1952**, *56*, 575.

(36) Piacentini, R.; Alfano, O.; Albizzati, E.; Luccini, E.; Herman, J. Solar Ultraviolet Irradiance for Clear Sky Days Incident at Rosario, Argentina: Measurements and Model Calculations. *J. Geophys. Res., D* **2002**, *107*, 6.

*Received for review* September 2, 2009
*Revised manuscript received* November 24, 2009
*Accepted* November 29, 2009

IE901377P